Characterization of band structure for transverse acoustic phonons in Fibonacci superlattices by a bandedge formalism

2008 J. Phys.: Condens. Matter 20 445224

(http://iopscience.iop.org/0953-8984/20/44/445224)

IOP PUBLISHING JOURNAL OF PHYSICS: CONDENSED MATTER

J. Phys.: Condens. Matter **20** (2008) 445224 (10pp) doi:10.1088/0953-8984/20/44/445224

Characterization of band structure for transverse acoustic phonons in Fibonacci superlattices by a bandedge formalism

W J Hsueh, R F Chen and K Y Tang

Department of Engineering Science, National Taiwan University, 1, Section 4, Roosevelt Road, Taipei 10660, Taiwan

E-mail: hsuehwj@ntu.edu.tw

Received 24 April 2008, in final form 8 September 2008
Published 10 October 2008
Online at stacks.iop.org/JPhysCM/20/445224

Abstract

We present a divergence-free method to determine the characteristics of band structures and projected band structures of transverse acoustic phonons in Fibonacci superlattices. A set of bandedge equations is formulated to solve the band structures for the phonon instead of using the traditional dispersion relation. Numerical calculations show band structures calculated by the present method for the Fibonacci superlattice without numerical instability, which may occur in traditional methods. Based on the present formalism, the band structure for the acoustic phonons has been characterized by closure points and the projected bandgaps of the forbidden bands. The projected bandgaps are determined by the projected band structure, which is characterized by the cross points of the projected bandedges. We observed that the band structure and projected band structure and their characteristics were quite different for different generation orders and the basic layers for the Fibonacci superlattice. In this study, concise rules to determine these characteristics of the band structure and the projected band structure, including the number and the location of closure points of forbidden bands and those of projected bandgaps, in Fibonacci superlattices with arbitrary generation order and basic layers are proposed.

(Some figures in this article are in colour only in the electronic version)

1. Introduction

Heterostructures and superlattices have been extensively studied for their potential applications in modern electronic and optoelectronic systems. The behavior of phonons scattering and coupling in the superlattices has received much attention for developing high frequency nanostructured devices. Of these researches, periodic superlattices with a two-layer basis, including band structures in the completely periodic superlattices [1–12], surface phonons in semi-infinite superlattices [13–15], localized modes in the superlattices with cavities [16–22] and eigenstates in finite superlattices [23–26] have been very well studied. Recently, quasi-periodic superlattices, especially for Fibonacci systems, have received a great deal of interest [17–20]. The Fibonacci superlattices are made of two basic layers under the configuration of the Fibonacci sequence. The property of phonons propagating in these systems is quite different from that in the periodic or random ones.

Acoustic phonons with shear horizontal polarization propagating in infinite, semi-infinite and finite superlattices have received much interest in recent years [5–8, 13, 15]. An accurate determination of band structures plays an important role in the study of phonons in the superlattices. In completely periodic systems, band structures show the allowed and forbidden bands of the phonon propagation. Moreover, for semi-infinite and defect superlattices, band structure can offer an important reference for examining the localized surface and defect states, which should be located in the forbidden band. Even for finite superlattices, the transmission resonance and localization of phonons exist in the allowed band of the band structure.

Band structures of phonons in superlattices can be determined by the dispersion relation, which is obtained by

the eigenenergy equation. As the generation orders of the Fibonacci superlattice are 2 and 3, the superlattices can be treated by bilayer periodic structures. As we know, the dispersion relation for bilayer superlattices can be expressed in the concise Kronig–Penney form [5, 7]. When the generation orders of the Fibonacci superlattices are greater than three, the band structure is usually calculated by numerical methods [4, 15, 20–28] because of difficulty in deriving the required analytical expressions. For these multiple basis superlattices, several numerical methods have been proposed for calculating the band structure. Of these methods, the transfer matrix method is the most popular because it is easy to calculate the dispersion relation by trace operation of the global matrix. However, numerical instability may occur in calculating the dispersion relation.

The band structure of acoustic phonon propagation in Fibonacci superlattices depends on the parameters of two basic layers as well as the generation order [16–22]. Since the variation of the band structure seems complicated for simultaneous variation of the basic layers and the generation order, most investigations have addressed the effect for different generation orders based on a few sets of basic layers. However, as the basic layers are changed, the pattern of the band structure may significantly differ in irregularity even for bilayer systems. Thus, it is difficult to determine the characteristics of the band structure for arbitrary generation order and basic layers according to the studies for different generation order under a few fixed basic layers. As we know, studies of the characteristics of the band structure in the Fibonacci superlattice affected by simultaneous change in the basic layers and the generation order are limited.

In this paper, a novel numerically stable method based on graph theory is presented to understand the characteristics of the band structures of acoustic phonons with shear horizontal polarization in Fibonacci superlattices. Graph theory has been applied to analyze networks and linear systems [29–31]. However, to the best of our knowledge, graph theory has not been applied to research acoustic phonons in superlattices. Based on graph theory, a bandedge equation is drawn up in this paper to calculate the band structure in Fibonacci superlattices to avoid numerical instability. In this study, the characteristics of the band structure for the Fibonacci superlattice with different generation order and basic layers are investigated. Moreover, we propose the relationship between the pattern of the band structure and the projected band structure. Based on the relation, the characteristics of the band structure of the acoustic phonon in the Fibonacci superlattice with arbitrary generation order and arbitrary basic layers can be determined according to the pattern of the projected band structures.

2. Basic theory and formulation

We consider the transverse acoustic phonons propagating in a one-dimensional periodic superlattice, in which each unit cell is composed of two kinds of materials A and B with the structure following the Fibonacci sequence as

$$S_{\nu+1} = \{S_{\nu-1}S_{\nu}\}, \tag{1}$$

with $S_0 = \{B\}$ and $S_1 = \{A\}$. In this study, materials A and B are considered isotropic or cubic crystals.

For the isotropic material, the displacement field of the transverse acoustic phonons u_2 along the x_2 axis and the wavevector of phonons k in the (x_1, x_3) plane are considered. According to the elastic equation of motion, the displacement in layer j is given by

$$\frac{\partial^2 u_2(j, x_1, x_3, t)}{\partial t^2} = \left[\frac{\partial^2}{\partial x_1^2} + \frac{\partial^2}{\partial x_3^2}\right] c_{t,j}^2 u_2(j, x_1, x_3, t), \tag{2}$$

where $c_{t,j}$ is the velocity of the transverse acoustic phonons. For the cubic crystal, we consider the crystal with (001) in the direction of the interfaces of each layer. Thus the equation of motion of the displacement is

$$\left[\frac{\partial^2}{\partial x_1^2} + \frac{\partial^2}{\partial x_3^2}\right] C_{44,j} u_2 + \rho_j \frac{\partial^2 u_2}{\partial t^2} = 0, \tag{3}$$

where $C_{44,j}$ and ρ_j are the elastic constant and mass density, respectively. Equation (3) can be reduced to equation (2) with $c_{t,j} = (C_{44,j}/\rho_j)^{1/2}$. To reduce the analysis work, we define a wavevector $k_{\|}$ along [100] without losing generality.

For the propagating modes, the displacement in layer j of a cell is described by

$$u_2(j, x_1, x_3, t) = u_2(j, x_1)\exp(\mathrm{i}\omega t - \mathrm{i}k_{\|}x_3). \tag{4}$$

The solution of the displacement field in the layer can be represented by the summation of a forward and a backward traveling wave. Let the displacement at the boundary of the left and the right boundaries of the layer be U_{j-1} and U_j, respectively. The displacement field in the layer is expressed by

$$u_2(j, x_1) = \frac{1}{\sin k_j d_j}\Big[U_{j-1}\sin k_j(x_{1,j} - x_1) + U_j \sin k_j(x_1 - x_{1,j-1})\Big], \tag{5}$$

where k_j is the transverse wavevector, defined by $k_j = \pm(\omega^2/c_{t,j}^2 - k_{\|}^2)^{1/2}$. Since only the component of stress p_{12} in each layer is not zero, p_{12} in layer j is given by $\rho c_{t,j}^2(\partial u_2/\partial x_1)$. We can express the stress by the displacement field as

$$p_{12}(j, x_1) = \frac{\rho_j c_{t,j}^2 k_j}{\sin(k_j d_j)}\Big[-\cos k_j(x_{1,j} - x_1)U_{j-1} + \cos k_j(x_1 - x_{1,j-1})U_j\Big]. \tag{6}$$

From equations (5) and (6), we see that the displacement and stress fields at the left and right boundaries of the layer are dependent. The boundary conditions at the interface between two neighboring layers are the continuities of the displacement and the normal components of the stress. At the interface between layers j and $j+1$, the boundary conditions are

$$u_2(j, x_{1,j}) = u_2(j+1, x_{1,j}), \tag{7}$$

$$p_{12}(j, x_{1,j}) = p_{12}(j+1, x_{1,j}). \tag{8}$$

Here, we define a normalized stress variable $\bar{P}_j$ corresponding to the stress field at the right boundary of layer j as

$$\bar{P}_j = p_{12}(j, x_{1,j})D/(\rho_r c_{t,r}^2), \tag{9}$$

where D is the width of a cell, and ρ_r and $c_{t,r}$ are the mass density and wave velocity of a reference media. Thus, the relationship between the displacement and stress fields at the left and right boundaries of the layer may be written as

$$U_j = f_j U_{j-1} + h_j \bar{P}_j, \tag{10}$$

$$\bar{P}_{j-1} = f_j \bar{P}_j + g_j U_{j-1}, \tag{11}$$

where $f_j = \sec k_j d_j$, $g_j = (\rho_j c_{t,j}^2 k_j D \tan k_j d_j)/(\rho_r c_{t,r}^2)$, and $h_j = (\rho_r c_{t,r}^2 \tan k_j d_j)/(\rho_j c_{t,j}^2 k_j D)$.

According to equations (10) and (11), we represent the relations of U_{j-1}, U_j, $\bar{P}_{j-1}$ and $\bar{P}_j$ as a two-way graph model as shown in figure 1 [29]. For this particular modeling, phonons in a cell with N layers can be represented by a lead type model. Thus, the fields U_N and $\bar{P}_0$ depend on the fields U_0 and $\bar{P}_N$ represented by

$$U_N = f U_0 + h \bar{P}_N, \tag{12}$$

$$\bar{P}_0 = g U_0 + f \bar{P}_N, \tag{13}$$

where f, g, and h are $\prod_{j=1}^{N} f_j/S^{1,N}$, $(S^{1,N})^{-1}\sum_{p=1}^{N} S^{p,N} g_p \prod_{j=1}^{p-1} f_j^2$ and $(S^{1,N})^{-1}\sum_{p=1}^{N} S^{1,p} h_p \prod_{j=p+1}^{N} f_j^2$, respectively, and $S^{p,q}$ is the determinant for the graph from layer p to q. We can obtain $S^{p,q}$ using the topology method based on the graph for a cell and represent it as [29, 30]

$$S^{p,q} = \sum_{s=0}^{q-p} \sum_{i_{2s}=p+s}^{q} \sum_{i_{2s-1}=p+s-1}^{i_{2s}-1} \cdots \times \sum_{i_2=p+1}^{i_3} \sum_{i_1=p}^{i_2-1} \prod_{u=1}^{s} \left(-h_{i_{2u-1}} g_{i_{2u}} \prod_{j=i_{2u-1}}^{i_{2u}} f_{i_{2u}}^2 \right). \tag{14}$$

For the periodical structure, the displacement and stress fields in the superlattice must obey the Bloch waves, given by $U_0 = U_N \exp(-\mathrm{i}\phi)$ and $\bar{P}_N = \bar{P}_0 \exp(\mathrm{i}\phi)$. Based on the representations of Bloch waves, we obtain a new dispersion relation as

$$f^2 - 2f\cos\phi - gh + 1 = 0. \tag{15}$$

When $|\cos\phi| \leqslant 1$, the Bloch phase ϕ is a real value. In this condition, acoustic phonons propagating in the media are allowed and termed as the allowed band. When $|\cos\phi| > 1$, ϕ is complex. Thus, acoustic phonons are evanescent and termed as the forbidden band. At the bandedges of the forbidden band, the value of $\cos\phi$ is equal to 1 or -1. Thus, the new dispersion relation for the bandedges is rewritten by

$$J_e = 0 \qquad \text{for } e = 1, -1, \tag{16}$$

where J_e is the bandedge function defined by $J_e = f^2 - 2ef + 1 - gh$. Equation (16) is called the bandedge equation. Moreover, the center of the allowed band can be written as $J_0 = 0$. Using these equations, it is easy to determine the bandgaps and the band structures without calculating $\cos\phi$.

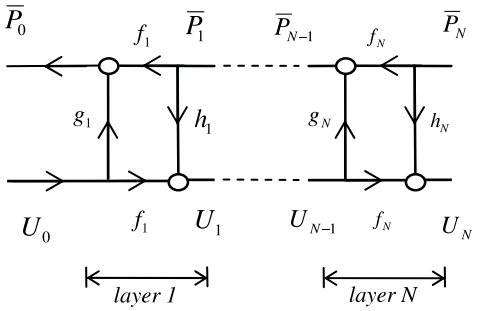

Figure 1. Graph model for the acoustic phonon in a superlattice with N layers.

3. Band structures in Fibonacci superlattices

For the Fibonacci superlattices, the band structure of the transverse acoustic phonons depends on two basic layers and the generation order. To interpret the effects of the materials and structures of the basic layers on the band structure in the superlattices, two types of materials for the basic layers are analyzed by the present method. First, we consider that the basic layers of the Fibonacci superlattice are made of Nb (A) and Fe (B), called type I. The parameters for type I superlattices are $C_{44,\mathrm{Nb}} = 2.87 \times 10^{10}$ N m^{-2}, $\rho_{\mathrm{Nb}} = 8.57 \times 10^3$ kg m^{-3}, $C_{44,\mathrm{Fe}} = 1.18 \times 10^{11}$ N m^{-2} and $\rho_{\mathrm{Fe}} = 7.8 \times 10^3$ kg m^{-3}. According to the Fibonacci generation schemes given in equation (1), we have $S_2 = \{BA\}$, $S_3 = \{ABA\}$, $S_4 = \{BAABA\}$, etc. The number of layers in a vth-generation Fibonacci superlattice N_v can be calculated by recursive form $N_{v+1} = N_v + N_{v-1}$ with $N_1 = 1$ and $N_2 = 2$. The numbers of layers A and B in S_v superlattices are N_{v-1} and N_{v-2}, respectively.

Using the present method, the band structures for a type I superlattice with S_4 basis is calculated and shown in figure 2, in which the widths of the basic layers are $d_{\mathrm{Nb}} = d_{\mathrm{Fe}} = 10$ nm, and the reduced frequency Ω is defined by $\Omega = \omega D/c_{t,\mathrm{Fe}}$. In this figure, the dispersion curves break up into different bands, in which the dark and white areas are the allowed and forbidden regions, respectively. The band structure is determined by the bandedge equations, equation (16), with $e = 1$ and -1 and represented by the solid and dotted lines, respectively. It indicates that the edges of odd and even bandgaps correspond to the roots of $J_1 = 0$ and $J_{-1} = 0$, respectively. All the allowed and forbidden bands are located in the region of $k_\parallel D < \omega D/c_{t,\mathrm{Nb}}$. As the wavevector $k_\parallel D$ increases, the width of each bandgap may reduce to zero and then increase. The asymptote line of each bandgap for infinite frequency approaches $k_\parallel D = \omega D/c_{t,\mathrm{Nb}}$, which is denoted by line L_{Nb} in the figure. The additional characteristics of the band structure are the band structure at $k_\parallel D = 0$ and the location of the closure points of each forbidden band. The band structure for the acoustic phonon in the Fibonacci superlattice can be estimated if these characteristics are known. However, the additional characteristics of the band structure depend on the basic layers and the generation order of the superlattice.

One of the closure points of each forbidden band, marked by an open circle in the figure, has been located on a straight

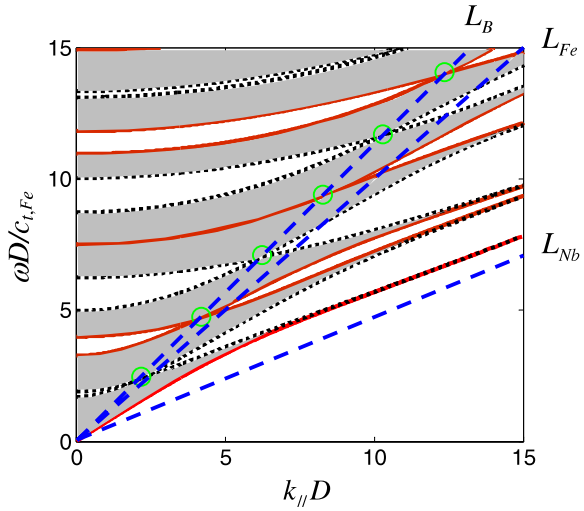

Figure 2. Band structure of the acoustic phonons propagating in the type I Fibonacci superlattice with fourth generation versus the wavevector $k_{\|}D$. Calculations are performed with $d_{\mathrm{Nb}} = d_{\mathrm{Fe}} = 10$ nm. Solid and dotted lines show the roots of $J_{+1} = 0$ and $J_{-1} = 0$, respectively. The dark area presents the allowed regions. Dashed lines L_{Fe}, L_{Nb} and L_{B} present the relation of $k_{\|}D = \omega D/c_{t,\mathrm{Fe}}$, $k_{\|}D = \omega D/c_{t,\mathrm{Nb}}$ and the Brewster line, respectively. The open circle indicates the Brewster points.

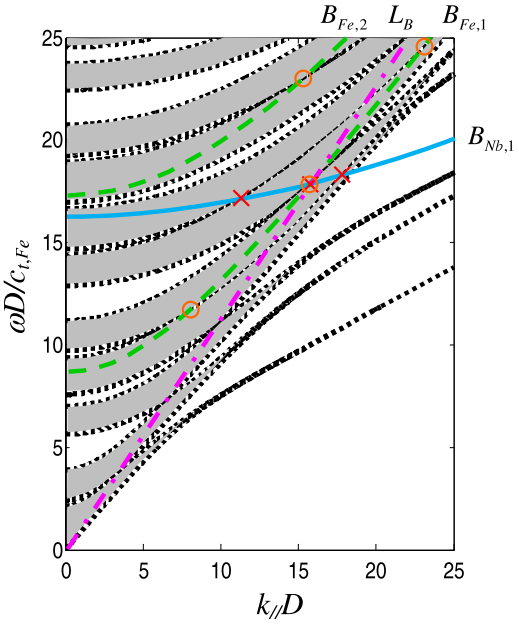

Figure 3. Closure points of bandgaps for the acoustic phonons in the type I Fibonacci superlattice with the fourth generation versus the wavevector $k_{\|}D$. Calculations are performed with $d_{\mathrm{Nb}} = 4$ nm and $d_{\mathrm{Fe}} = 16$ nm. The dotted lines show the edge of the bandgaps. The solid lines $B_{\mathrm{Nb},m}$ represent the roots of $k_{\mathrm{Nb}}d_{\mathrm{Nb}}(F) = m\pi$. The dashed lines $B_{\mathrm{Fe},n}$ represent the roots of $k_{\mathrm{Fe}}d_{\mathrm{Fe}}(F) = n\pi$. The dashed–dotted line L_{B} represents the Brewster line. The cross and open circles indicate the closure points of bandgaps on lines $B_{\mathrm{Nb},m}$ and $B_{\mathrm{Fe},n}$, respectively.

line L_{B} with a constant slope, which is analogous to the Brewster line in optics [6]. As the incident angle of the phonon is identical to the one corresponding to the acoustic Brewster line, the reflection of the phonon either from layer A to layer B or from layer B to layer A vanishes. The Brewster angle can be derived by zeroing the transmission coefficient of the phonon propagating as

$$\frac{\omega}{k_{\|}c_{t,A}} = \left\{ \frac{(\rho_A c_{t,A}^2)^2 - (\rho_B c_{t,B}^2)^2}{c_{t,A}^2[(\rho_A c_{t,A})^2 - (\rho_B c_{t,B})^2]} \right\}^{1/2}. \qquad (17)$$

From equation (17), we see that the Brewster line depends on the materials of basic layers A and B but is independent of the structure of the superlattice, including the widths of the basic layers and the generation order of the Fibonacci system.

As the widths of the basic layers are changed to $d_{\mathrm{Nb}} = 4$ nm and $d_{\mathrm{Fe}} = 16$ nm, the band structure for the type I superlattice with S_4 basis is shown in figure 3. Since the materials of the basic layers consist of Nb and Fe, the slope of the Brewster line in figure 3 is the same as in figure 2. However, the patterns of the band structure for both cases are quite different, even if the materials and the generation order of both superlattices are the same.

According to the graph model for the Fibonacci superlattice, we note that the effect of each Fe layer on the bandedge function J_e can be neglected if the parameters of the graph model for the Fe layer are $g_{\mathrm{Fe}} = h_{\mathrm{Fe}} = 0$ and $f_{\mathrm{Fe}} = 1$. This condition can be expressed by

$$k_{\mathrm{Fe}}d_{\mathrm{Fe}} = n\pi, \qquad \text{where } n = 1, 2, 3, \ldots. \qquad (18)$$

We plot the roots of $k_{\mathrm{Fe}}d_{\mathrm{Fe}} = n\pi$, $n = 1, 2, 3$, etc, by solid lines, called line $B_{\mathrm{Fe},n}$, in figure 3. Since the S_v Fibonacci superlattice consists of N_{v-1} and N_{v-2} layers of Nb and Fe, the graph model for a cell in the superlattice can be reduced to that for N_{v-1} cascade layers of Nb. Then, the parameters f, g and h of the graph model for a cell of S_v Fibonacci superlattices can be reduced to $f = \sec N_{v-1}k_{\mathrm{Nb}}d_{\mathrm{Nb}}$, $g = (\rho_{\mathrm{Fe}}c_{t,\mathrm{Fe}}^2 k_{\mathrm{Fe}}D \tan N_{v-1}k_{\mathrm{Nb}}d_{\mathrm{Nb}})/(\rho_r c_{t,r}^2)$ and $h = (\rho_r c_{t,r}^2 \tan N_{v-1}k_{\mathrm{Nb}}d_{\mathrm{Nb}})/(\rho_{\mathrm{Fe}}c_{t,\mathrm{Fe}}^2 k_{\mathrm{Fe}}D)$. Based on equation (16), the edges of the projected bandgaps for the condition are reduced to $\cos N_{v-1}k_{\mathrm{Nb}}d_{\mathrm{Nb}}(F) \pm 1 = 0$ or expressed by

$$k_{\mathrm{Nb}}d_{\mathrm{Nb}} = \frac{m\pi}{N_{v-1}}, \qquad \text{where } m = 1, 2, 3, \ldots. \qquad (19)$$

Thus, solutions of $N_{v-1}k_{\mathrm{Nb}}d_{\mathrm{Nb}} = m\pi$ and $k_{\mathrm{Fe}}d_{\mathrm{Fe}} = n\pi$, $m, n = 1, 2, 3$, etc,, are located on the closure points of projected bandgaps as marked by $C(m/N_{v-1}, n)$ in figure 3. It is noted that the lines of $k_{\mathrm{Fe}}d_{\mathrm{Fe}} = n\pi$ are denoted by $B_{\mathrm{Fe},n}$. The width ratio and the reduced frequency at the closure point $C(m/N_{v-1}, n)$ can be solved by the conditions of $k_{\mathrm{Nb}}d_{\mathrm{Nb}} = m\pi/N_{v-1}$ and $k_{\mathrm{Fe}}d_{\mathrm{Fe}} = n\pi$ and represented by

$$k_{\|}D = \frac{\pi}{1-\sigma^2}\left[N_{v-1} + \left(\frac{1-F}{F}\right)N_{v-2}\right] \times \left[\left(\frac{m\sigma}{N_{v-1}}\right)^2 - n^2\left(\frac{F}{1-F}\right)^2\right]^{1/2}, \qquad (20)$$

$$\frac{\omega D}{c_{t,\mathrm{Fe}}} = \frac{\sigma^2\pi}{(1-\sigma^2)^{1/2}}\left[N_{v-1} + \left(\frac{1-F}{F}\right)N_{v-2}\right] \times \left[\left(\frac{m}{N_{v-1}}\right)^2 - n^2\left(\frac{F}{1-F}\right)^2\right]^{1/2}, \quad (21)$$

where σ and F are the ratio of acoustic velocity and the width ratio of the basic layers, defined by $\sigma = c_{t,\mathrm{Nb}}/c_{t,\mathrm{Fe}}$ and $F = d_{\mathrm{Nb}}/(d_{\mathrm{Fe}} + d_{\mathrm{Nb}})$, respectively.

In the same way, if $k_{\mathrm{Nb}}d_{\mathrm{Nb}} = m\pi$, $m = 1, 2, 3$, etc, the graph model for a cell of the S_v Fibonacci superlattice can be reduced to that for N_{v-2} cascade Fe layers. Thus, the bandedge equation is reduced to $\cos N_{v-2}k_{\mathrm{Fe}}d_{\mathrm{Fe}} \pm 1 = 0$. The cross point between the lines of $k_{\mathrm{Nb}}d_{\mathrm{Nb}} = m\pi$ and $N_{v-2}k_{\mathrm{Fe}}d_{\mathrm{Fe}} = n\pi$, $m, n = 1, 2, 3$, etc, will be located on the closure point of the projected bandgap and marked by $C(m, n/N_{v-2})$ in figure 3. According to $k_{\mathrm{Nb}}d_{\mathrm{Nb}} = m\pi$ and $k_{\mathrm{Fe}}d_{\mathrm{Fe}} = n\pi/N_{v-2}$, the width ratio and the reduced frequency for the closure point $C(m, n/N_{v-2})$ can be solved as

$$k_\parallel D = \frac{\pi}{1-\sigma^2}\left[N_{v-1} + \left(\frac{1-F}{F}\right)N_{v-2}\right] \times \left[(m\sigma)^2 - \left(\frac{n}{N_{v-2}}\right)^2\left(\frac{F}{1-F}\right)^2\right]^{1/2}, \quad (22)$$

$$\frac{\omega D}{c_{t,\mathrm{Fe}}} = \frac{\sigma^2\pi}{(1-\sigma^2)^{1/2}}\left[N_{v-1} + \left(\frac{1-F}{F}\right)N_{v-2}\right] \times \left[m^2 - \left(\frac{n}{N_{v-2}}\right)^2\left(\frac{F}{1-F}\right)^2\right]^{1/2}. \quad (23)$$

From these results, we conclude that all closure points of each forbidden band for type I of the S_v superlattice are located on the Brewster line or lines $B_{\mathrm{Nb},m}$, $B_{\mathrm{Fe},n}$, for $m, n = 1, 2, 3$, etc. However, the locations of these closure points are complicated since the values of $k_\parallel D$ and $\omega D/c_{t,\mathrm{Fe}}$ depend not only on the generation order v of the superlattice but also on the parameters for two basic layers. Moreover, the characteristics of the band structure include not only the closure points of the forbidden band but also the band structure at $k_\parallel D = 0$. Unfortunately, the location and width of bandgaps at $k_\parallel D = 0$ of the band structure also depend on the generation order or the basic layers. Thus it is difficult to see the variation of the band structure induced by changing the parameters of the Fibonacci superlattice.

The frequency of the Brewster points in each forbidden band of the superlattices versus the width ratio F is shown in figure 4, in which the generation orders 2, 3, 4, 5 and 6 of the Fibonacci superlattice are presented. We see that the location of the Brewster point in each forbidden band differs for different widths of the two basic layers although the Brewster line for the superlattice is not changed. It is noted that the frequency of the Brewster point of a Fibonacci superlattice depends on the width ratio F of the basic layers but is independent of the total width D of a cell in the superlattice. As the width of layer Nb approaches zero, the reduced frequencies of the Brewster points reach $\omega D/c_{t,\mathrm{Fe}} = 6.675$, 13.35 and 20.05 for forbidden bands 1, 2 and 3, respectively. If the width of layer Fe approaches zero, the reduced frequencies of the Brewster points for the forbidden bands 1, 2 and 3 reach

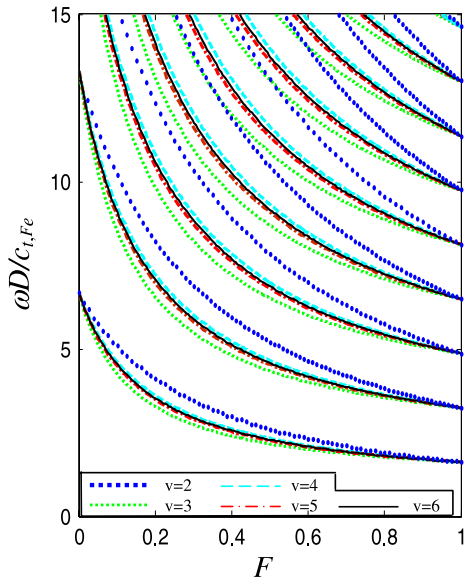

Figure 4. Reduced frequency of the Brewster point of each forbidden band versus the width ratio $0 < F < 1$ for the acoustic phonons in the S_v Fibonacci superlattice.

$\omega D/c_{t,\mathrm{Fe}} = 1.625$, 3.25 and 4.875, respectively. It is observed that the Brewster points for the superlattice with generation order $v = 4$ are located between those for $v = 2$ and 3, and the Brewster points for $v = 5$ is located between those for $v = 3$ and 4. We find that the Brewster points for the superlattice with generation order v are located between that for generation order $v - 1$ and $v - 2$, and converged for higher v.

Next, we study the projected bandgap structure of the acoustic phonon in the superlattice. The projected bandgap is defined as the bandgap of the forbidden band by zeroing the wavevector in the direction perpendicular to the layer surface, $k_\parallel D = 0$. The projected bandgap structure for the Fibonacci superlattices with the generation order 2–5, respectively, versus the width ratio F is shown in figures 5(a)–(d), in which dotted lines mark the edges of each projected bandgap. We see that the width of all gaps vanish at the same frequency for the condition $F = 0$ and 1.0 of the superlattice with different generation orders. When the width ratio approaches zero, the reduced frequencies of the gap centers reach $\omega D/c_{t,\mathrm{Fe}} = \pi, 2\pi, 3\pi, \ldots$. Moreover, as the width ratio approaches one, the reduced frequencies of the gap centers reach $\omega D/c_{t,\mathrm{Fe}} = \pi c_{t,\mathrm{Nb}}/c_{t,\mathrm{Fe}}, 2\pi c_{t,\mathrm{Nb}}/c_{t,\mathrm{Fe}}, 3\pi c_{t,\mathrm{Nb}}/c_{t,\mathrm{Fe}}, \ldots$.

For nonzero width ratio $F \neq 0$, the closure points of each projected bandgap can be analyzed by the same method for calculating the closure points of the forbidden band in the band structure. However, the wavevector of the acoustic phonon in the projected band structure is not a function of the perpendicular wavevector $k_\parallel$. Moreover, the widths of the basic layers are changed for different F. If $k_{\mathrm{Fe}}d_{\mathrm{Fe}}(F) = n\pi$, $n = 1, 2, 3$, etc, the parameters f_{Fe}, g_{Fe} and h_{Fe} of the graph model become 1, 0 and 0, respectively. The graph model for a cell of the superlattice can be reduced to that for N_{v-1} cascade layers of Nb. The cross points between lines of $N_{v-1}k_{\mathrm{Nb}}d_{\mathrm{Nb}}(F) = m\pi$ and $k_{\mathrm{Fe}}d_{\mathrm{Fe}}(F) = n\pi$, $m, n = 1, 2, 3$, etc, will be located on the closure points of the projected

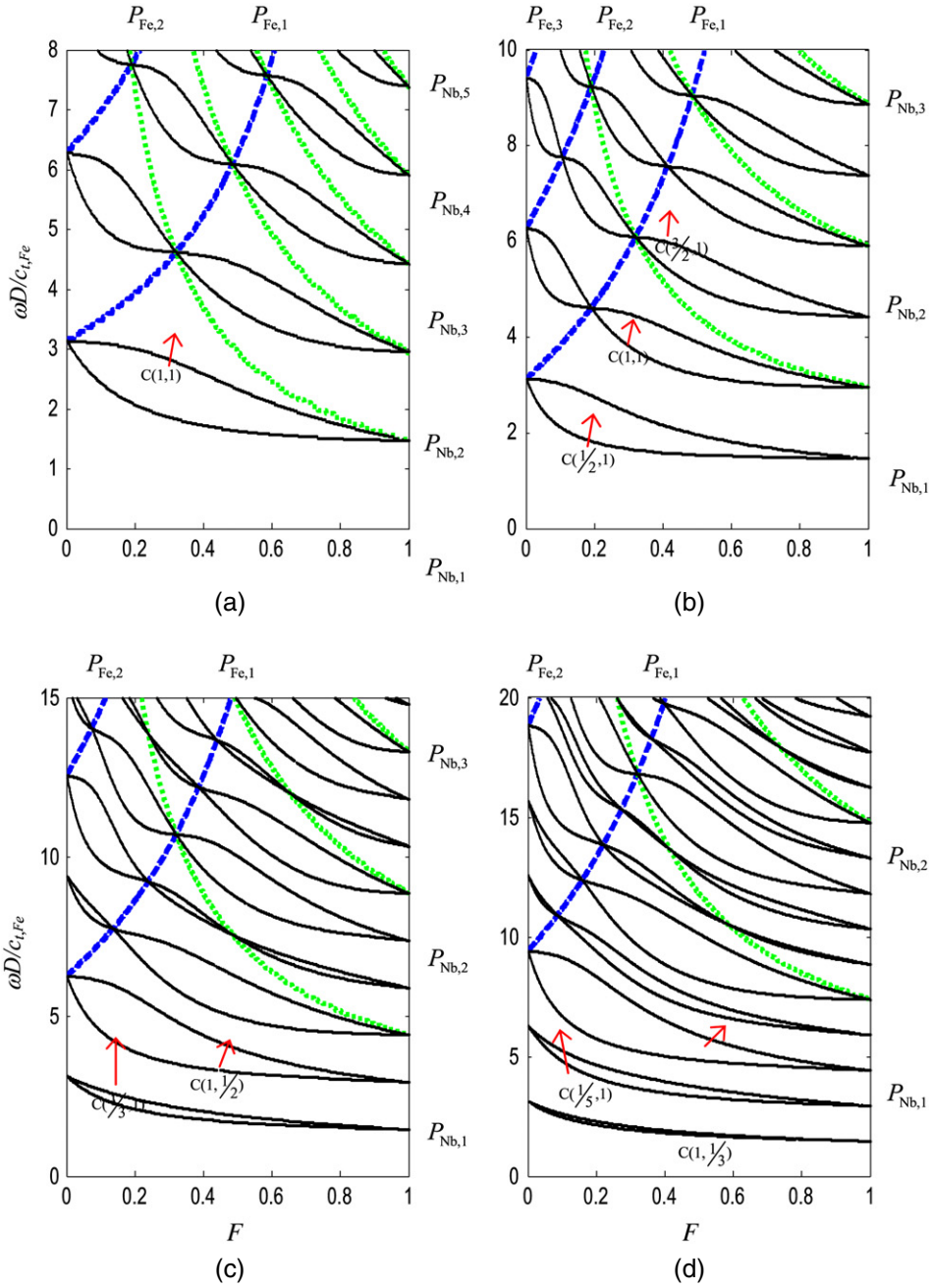

Figure 5. Projected band structure versus the width ratio F for the acoustic phonons in the S_v type I Fibonacci superlattice. (a) $v = 2$, (b) $v = 3$, (c) $v = 4$ and (d) $v = 5$. The solid line represents the edges of the bandgaps. The dotted lines $P_{\mathrm{Nb},m}$ represent the roots of $k_{\mathrm{Nb}}d_{\mathrm{Nb}}(F) = m\pi$. The dashed lines $P_{\mathrm{Fe},n}$ represent the roots of $k_{\mathrm{Fe}}d_{\mathrm{Fe}}(F) = n\pi$.

bandgaps marked by $C(m/N_{v-1}, n)$ in figure 5, in which lines of $k_{\mathrm{Nb}}d_{\mathrm{Nb}}(F) = m\pi$ and $k_{\mathrm{Fe}}d_{\mathrm{Fe}}(F) = n\pi$ are denoted by $P_{\mathrm{Nb},m}$ and $P_{\mathrm{Fe},n}$, respectively. The width ratio and the reduced frequency at the closure point $C(m/N_{v-1}, n)$ can be solved as

$$F = \frac{m\sigma}{nN_{v-1} + m\sigma}, \tag{24}$$

$$\frac{\omega D}{c_{t,\mathrm{Fe}}} = (nN_{v-2} + m\sigma)\pi. \tag{25}$$

In the same way, if $k_{\mathrm{Nb}}d_{\mathrm{Nb}}(F) = m\pi$, $m = 1, 2, 3$, etc, for nonzero width ratio $F \neq 0$, the bandedge equation for the S_v Fibonacci superlattice is reduced to $\cos N_{v-2}k_{\mathrm{Fe}}d_{\mathrm{Fe}}(F) \pm 1 = 0$. The cross point between lines of $k_{\mathrm{Nb}}d_{\mathrm{Nb}}(F) = m\pi$ and $N_{v-2}k_{\mathrm{Fe}}d_{\mathrm{Fe}}(F) = n\pi$, $m, n = 1, 2, 3$, etc, will be located on the closure point of the projected bandgap and marked by $C(m, n/N_{v-2})$ in figure 5. The width ratio and the reduced frequency for the closure point $C(m, n/N_{v-2})$ can be solved as

$$F = \frac{mN_{v-2}\sigma}{n + mN_{v-2}\sigma}, \tag{26}$$

Table 1. The values of $M^{(4)}_{A,j}$, $M^{(4)}_{B,j}$ and $M^{(4)}_{j}$ for calculating the total number of closure points in projected bandgap j within the range of $0 < F < 1$ for the Fibonacci superlattice with generation order 4.

No. of projected gap	Number of closure points		
	$M^{(4)}_{A,j}$	$M^{(4)}_{B,j}$	$M^{(4)}_{j}$
1	0	0	0
2	0	0	0
3	0	1	1
4	1	1	2
5	0	2	2
6	1	2	3
7	1	3	4
8	1	3	4
9	1	4	5
10	2	4	6
11	1	5	6
12	2	5	7
13	2	6	8
14	2	6	9

$$\frac{\omega D}{c_{t,\mathrm{Fe}}} = (n + mN_{v-1}\sigma)\pi. \tag{27}$$

From figures 5(a)–(d), we conclude that all the closure points of each projected bandgap are located on the lines $P_{\mathrm{Nb},m}$ or $P_{\mathrm{Fe},n}$, for $m, n = 1, 2, 3$, etc, in each S_v superlattice.

According to the results given in figures 5(a)–(d), the number of closure points of each projected bandgap within the region of $0 < F < 1.0$ for type I superlattice can be calculated by

$$M^{(v)}_{j} = M^{(v)}_{A,j} + M^{(v)}_{B,j}, \tag{28}$$

where $M^{(v)}_{j}$ is the total number of closure points of projected bandgap j for the Fibonacci superlattice with generation order v. $M^{(v)}_{B,j}$ is the number of closure points on lines of $k_{\mathrm{Fe}}d_{\mathrm{Fe}}(F) = nN_{v-2}\pi$, $n = 1, 2, 3$, etc, $M^{(v)}_{A,j}$ is the number of the closure points only on the lines $k_{\mathrm{Nb}}d_{\mathrm{Nb}}(F) = mN_{v-1}\pi$ but not on the lines of $k_{\mathrm{Fe}}d_{\mathrm{Fe}}(F) = nN_{v-2}\pi$, $m, n = 1, 2, 3$, etc. Table 1 illustrates the number of closure points in each projected bandgap of the S_4 superlattice based on the present method and figure 5(c). We find that $M^{(v)}_{A,j}$ and $M^{(v)}_{B,j}$ for the S_v type I superlattice can be calculated by the following recursive form:

$$M^{(v)}_{A,j} = \begin{cases} M^{(v)}_{A,j-N_{v-1}} & \text{for } j > N_{v-1}, \\ & \text{and } \mathrm{Rem}(j/N_{v-1}) = N_{v-2} \\ M^{(v)}_{A,j-N_{v-1}} + 1 & \text{for } j > N_{v-1}, \\ & \text{and } \mathrm{Rem}(j/N_{v-1}) \neq N_{v-2} \end{cases} \tag{29}$$

$$M^{(v)}_{B,j} = M^{(v)}_{B,j-N_{v-2}} + 1 \qquad \text{for } j > N_{v-2}, \tag{30}$$

with $M^{(v)}_{A,1} = M^{(v)}_{A,2} = \cdots = M^{(v)}_{A,N_{v-1}} = 0$ and $M^{(v)}_{B,1} = M^{(v)}_{B,2} = \cdots = M^{(v)}_{B,N_{v-2}} = 0$. The function of Rem in equation (29) is the reminder operation.

Let us consider the case of S_4 and type I superlattice. From figure 5(c), we observed that the number of closure points of the projected bandgap within the region of $0.2 < F < 1.0$ for gap $j = 1, 2$, etc, denoted by $M^{(I,4)}_{j,0.2<F<1.0}$, is given in column 2 of table 2. According to the band structure of the superlattice with $F = 0.2$ as shown in figure 3, the number of closure points in forbidden band $l = 1, 2$, etc, of the band structure, denoted by $\bar{M}^{(I,4)}_{j,F=0.2}$, is shown in column 3 of table 2. Notably, the value of $M^{(I,4)}_{j,0.2<F<1.0}$ is equal to 1 subtracted from $\bar{M}^{(I,4)}_{j,F=0.2}$ for $j = l = 1, 2$, etc. It indicates that for the S_v type I superlattices, the number of closure points in the forbidden band j of the band structure for width ratio F_1, except for the Brewster point, is identical to that of closure points in projected bandgap j within the region of $F_1 < F < 1.0$ expressed by

Table 2. Comparison between the total number of closure points in gap j of the projected band structure within the range of $0.2 < F < 1$ and that in forbidden band j of the band structure in the superlattice with $F = 0.2$ for type I and II of S_4 superlattices.

Gap no.	Type I superlattice		Type II superlattice	
	$M^{(I,4)}_{j,0.2<F<1.0}$	$\bar{M}^{(I,4)}_{j,F=0.2}$	$M^{(\mathrm{II},4)}_{j,0.2<F<1.0}$	$\bar{M}^{(\mathrm{II},4)}_{j,F=0.2}$
1	0	1	0	0
2	0	1	0	0
3	0	1	0	0
4	2	3	1	1
5	1	2	1	1
6	2	3	1	1
7	2	3	2	2
8	2	3	1	1
9	3	4	2	2
10	3	4	3	3
11	4	5	2	2
12	4	5	3	3

$$M^{(I,4)}_{j,0.2<F<1.0} = \bar{M}^{(I,4)}_{j,F=0.2} - 1. \tag{31}$$

The band structure in figures 2 and 3 and the projected bandgap in figure 5 can also be determined by the traditional method according to the values of $\cos\phi$. A comparison of the numerical stability of calculation by the present and the traditional methods is performed. We first consider an S_8 type I superlattice with $d_{\mathrm{Fe}} = d_{\mathrm{Nb}} = d = 10$ nm: the upper bounds of the band structure calculations using the present method and the traditional method for various frequencies ω are compared in figure 6. In the example, the maximum absolute values of J_{+1}, J_{-1}, J_0, f, g and h for the present method and $\cos\phi$ for the traditional method are also considered. Since the amplitude of the acoustic phonon decays for the condition of $k_{\|}D > \omega D/c_{t,\mathrm{Nb}}$, the allowed bands should be located on the left-hand side of the line $k_{\|}D = \omega D/c_{t,\mathrm{Nb}}$, as shown in figures 2 and 3. Thus, the range for calculation by both methods is also considered under $0 < k_{\|}D < \omega D/c_{t,\mathrm{Nb}}$. From the figure, we find that the upper bound of the calculation in the range by our method is almost constant for different frequencies but the upper bound by the traditional method is enlarged exponentially by increasing the frequency.

We next study the band structure in the Fibonacci superlattices with different generation orders by the present and traditional methods. The calculation is examined by both methods for a given frequency, $\omega d/c_{t,\mathrm{Fe}} = 2$, in the range of $0 < k_{\|}D < \omega D/c_{t,\mathrm{Nb}}$. These are type I superlattices with $d_{\mathrm{Fe}} = d_{\mathrm{Nb}} = d = 10$ nm for each generation order.

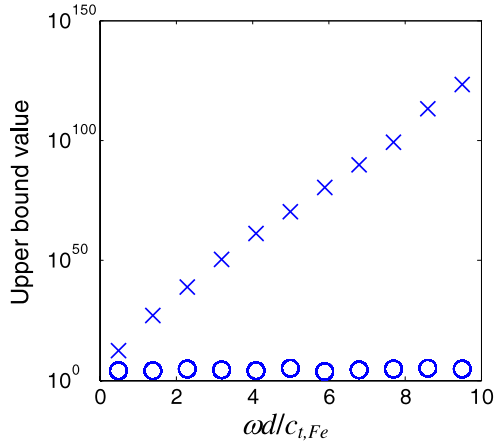

Figure 6. Comparison of the upper bounds versus frequencies in calculating the band structure by the present and traditional methods for a Fibonacci superlattice with eighth generation. The range considered in the traditional method is only $0 < k_{\|}D < \omega D/c_{t,\mathrm{Nb}}$, but that in the present method is extended to $k_{\|}D > 0$. The circle and the cross pattern presents the maximum absolute values of the calculations in the present method and the traditional method, respectively.

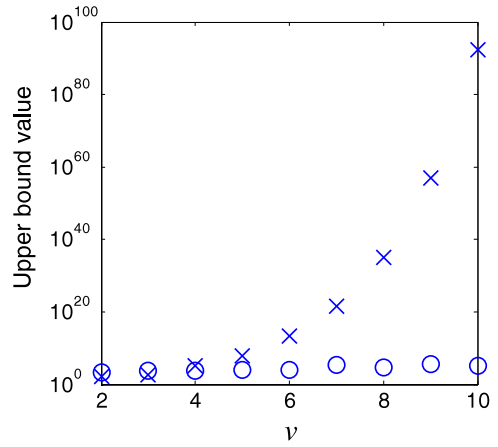

Figure 7. Comparison of the upper bounds in the band structure calculations by the present method and traditional method for the Fibonacci superlattice with vth generation at $\omega d/c_{t,\mathrm{Nb}} = 2$. The upper bound of the present method (circle) is considered by the maximum absolute value of $J_{\pm 1}$, J_0, f, g and h. The upper bound of the traditional method (cross) is considered by the maximum absolute value of $\cos(KL)$. The range considered in the traditional method is only $0 < k_{\|}D < \omega D/c_{t,\mathrm{Nb}}$, but that in the present method can be extended to $k_{\|}D > 0$.

Figure 7 shows a comparison of the maximum absolute values in the calculation by the present and traditional methods. We note that the upper bound in the traditional analysis increases exponentially for increasing generation order but does not enlarge for a higher generation order in the present method.

Next, we examine a Fibonacci superlattice consisting of elements Au (A) and Si (B). The material properties are $C_{44,\mathrm{Au}} = 4.17 \times 10^{10}$ N m^{-2}, $\rho_{\mathrm{Au}} = 1.932 \times 10^{10}$ kg m^{-3}, $C_{44,\mathrm{Si}} = 7.96 \times 10^{10}$ N m^{-2} and $\rho_{\mathrm{Si}} = 2.33 \times 10^{3}$ kg m^{-3}. The ratio of acoustic velocity σ and the width ratio of the basic layers F for the superlattice is defined by $\sigma = c_{t,\mathrm{Au}}/c_{t,\mathrm{Si}}$ and $F = d_{\mathrm{Au}}/(d_{\mathrm{Au}} + d_{\mathrm{Si}})$, respectively. Figure 8 provides the band structures of the transverse acoustic phonon in the Fibonacci superlattice with generation order 4, $d_{\mathrm{Au}} = 4$ nm and $d_{\mathrm{Si}} = 16$ nm ($F = 0.2$). The Brewster line does not exist in the band structure of this type of superlattice, called a type II superlattice. It is noteworthy that there are no closure points in the fundamental and second forbidden bands of the band structure in the superlattice. We observe that the slope of the Brewster line $\omega/k_{\|}c_{t,A}$ for the type II superlattice becomes imaginary. According to equation (17), if a Fibonacci superlattice with either $\rho_B c_{t,B}(\rho_A c_{t,A})^{-1} < 1$ and $\rho_B c_{t,B}^2(\rho_A c_{t,A}^2)^{-1} > 1$ or $\rho_B c_{t,B}(\rho_A c_{t,A})^{-1} > 1$ and $\rho_B c_{t,B}^2(\rho_A c_{t,A}^2)^{-1} < 1$, there are no Brewster points in the superlattice.

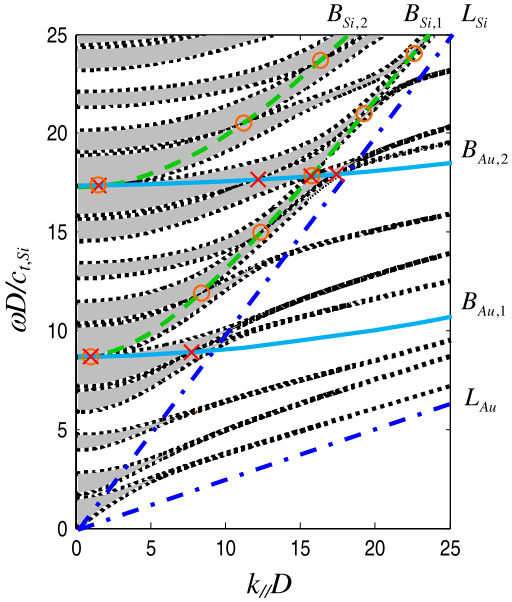

Figure 8. Band structures in the S_4 type II superlattice with $d_{\mathrm{Au}} = 4$ nm and $d_{\mathrm{Si}} = 16$ nm ($F = 0.2$). The dotted lines show the edge of the bandgaps. The solid lines $B_{\mathrm{Au},m}$ represent the roots of $k_{\mathrm{Au}}d_{\mathrm{Au}}(F) = m\pi$. The dashed line $B_{\mathrm{Si},n}$ represents the roots of $k_{\mathrm{Si}}d_{\mathrm{Si}}(F) = n\pi$. Dashed–dotted lines L_{Si} and L_{Au} represent the relation of $k_{\|}D = \omega D/c_{t,\mathrm{Si}}$ and $k_{\|}D = \omega D/c_{t,\mathrm{Au}}$, respectively. The cross and open circles indicate the closure points of bandgaps on lines $B_{\mathrm{Nb},m}$ and $B_{\mathrm{Fe},n}$, respectively.

The bandedges of each projected bandgap for the width ratio $0 < F < 1$ for S_4 type II superlattices is shown in figure 9. As the width ratio approaches zero, the reduced frequencies of cross points of each bandgap are equal to $\omega D/c_{t,\mathrm{Si}} = \pi$, 2π, 3π, etc. Moreover, as the width ratio approaches one, the reduced frequencies of the gap centers reach $\omega D/c_{t,\mathrm{Si}} = \pi c_{t,\mathrm{Au}}/c_{t,\mathrm{Si}}$, $2\pi c_{t,\mathrm{Au}}/c_{t,\mathrm{Si}}$, $3\pi c_{t,\mathrm{Au}}/c_{t,\mathrm{Si}}$, etc. We see that the pattern of the projected bandgap in the range of $0 < F < 1$ for the S_v Fibonacci superlattice of type II is similar to type I. The number of closure points in each of the bandgaps of the projected band structure for types I and II of the Fibonacci superlattices are identical and counted by equation (28) with equations (29) and (30).

Based on figure 9, the number of closure points in the range of $0.2 < F < 1.0$ for each projected bandgap, denoted by $M^{(\mathrm{II},4)}_{j,0.2<F<1.0}$, is illustrated in column 4 of table 2. Column 5

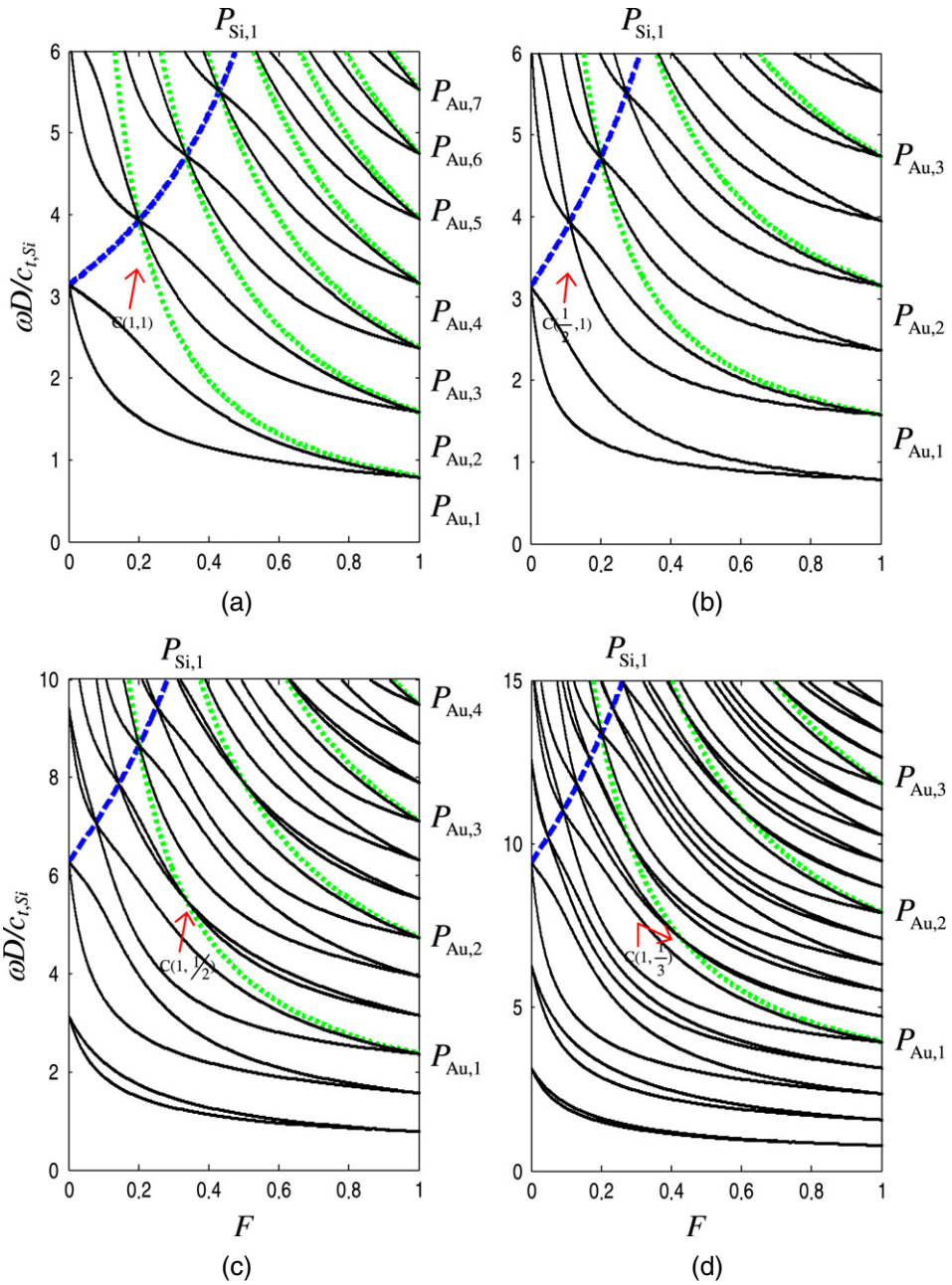

Figure 9. Projected band structure versus the width ratio F for the acoustic phonons in the S_v type II Fibonacci superlattice. (a) $v = 2$, (b) $v = 3$, (c) $v = 4$ and (d) $v = 5$. The solid line represents the edges of the projected bandgaps. The dotted line $P_{\mathrm{Au},m}$ and dashed line $P_{\mathrm{Si},n}$ correspond to the roots of $k_{\mathrm{Au}}d_{\mathrm{Au}}(F) = m\pi$ and $k_{\mathrm{Si}}d_{\mathrm{Si}}(F) = n\pi$, respectively.

of table 2 shows the number of closure points of each forbidden band in the band structures for $F = 0.2$, denoted by $\bar{M}^{(\mathrm{II},4)}_{j,F=0.2}$, which is counted from figure 8. It points out for the S_v type II superlattices, the number of the closure points in the forbidden band j of the band structure for width ratio F_1, except for the Brewster point, is identical to that of the closure points in the bandgap j of the projected band structure within the region of $F_1 < F < 1.0$, expressed by

$$M^{(\mathrm{II},4)}_{j,0.2<F<1.0} = \bar{M}^{(\mathrm{II},4)}_{j,F=0.2}. \tag{32}$$

From these results, we find that the number of closure points of each forbidden band in the band structures for a given width ratio F_1 depends on each projected gap within the range of $F_1 < F < 1.0$ based on the relation of equations (31) and (32) for the superlattice types I and II, respectively.

4. Conclusions

We have presented the band structure and projected band structure of the transverse acoustic phonons propagation in Fibonacci superlattices calculated by a bandedge equation. The bandedge equation is formulated by an analytical and concise form based on a graph theory. Numerical results show that computing the band structure for Fibonacci superlattices by

the traditional method may have numerical instability, but the present method is divergence-free.

The characteristics of the band structure of the acoustic phonons in Fibonacci superlattices, including the closure points and the projected gaps of each forbidden band, are quite different for changing generation orders or basic layers. It is interesting that the superlattice can be classified into two types, type I and type II, based on the materials of the basic layers. The patterns of projected band structures of type I and II superlattices are similar, but the band structures of both types are quite different. We find that the characteristics of the band structure for both types I and II can be determined by concise formulae and the projected band structure.

According to the present method, we can exactly determine the characteristics of the band structure and projected band structure for Fibonacci superlattices with arbitrary generation order and basic layers. Although only the materials Nb/Fe and Au/Si have been examined in this study, these obtained results can be extended to the superlattices made of other materials, such as semiconductors and compound semiconductors. In addition, the characteristics of the band structure and projected band structure can offer an important reference to studies of the transmission resonance, localized states, density of states, coupling of phonons and electron–phonon interaction for superlattices with various structures.

Acknowledgment

The authors acknowledge support from the National Science Council of Taiwan under grant no. NSC 95-2221-E-002-429.

References

[1] Tamura S, Hurley D C and Wolfe J P 1988 *Phys. Rev.* B **38** 1427
[2] Bargheer M, Zhavoronkov N, Gritsai Y, Woo J C, Kim D S, Woerner M and Elsaesser T 2004 *Science* **306** 1771
[3] Kini R N, Kent A J, Stanton N M and Henini M 2006 *Appl. Phys. Lett.* **88** 134112
[4] Rodriguez A, Noguera A, Szwacka T, Mendialdua J and Dobrzynski L 1989 *Phys. Rev.* B **39** 12568
[5] Camley R E, Djafari-Rouhani B, Dobrzynski L and Maradudin A A 1983 *Phys. Rev.* B **27** 7318
[6] Manzanares-Martinez B and Ramos-Mendieta F 2000 *Phys. Rev.* B **61** 12877
[7] Hammouchi M, El Boudouti E H, Nougaoui A, Djafari-Rouhani B, Lahlaouti M L H, Akjouj A and Dobrzynski L 1999 *Phys. Rev.* B **59** 1999
[8] El Boudouti E H and Djafari-Rouhani B 1994 *Phys. Rev.* B **49** 4586
[9] Tredicucci A, Gmachl C, Capasso F, Sivco D L, Hutchinson A L and Cho A Y 1998 *Nature* **396** 350
[10] Bartels A, Dekorsy T and Kurz H 1998 *Appl. Phys. Lett.* **72** 2844
[11] Pu N W and Bokor J 2003 *Phys. Rev. Lett.* **91** 076101
[12] Trigo M, Eckhause T A, Reason M, Goldman R S and Merlin R 2006 *Phys. Rev. Lett.* **97** 124301
[13] El Boudouti E H, Djafari-Rouhani B, Khourdifi E M and Dobrzynski L 1993 *Phys. Rev.* B **48** 10987
[14] Pilla O, Lemos V and Montagna M 1994 *Phys. Rev.* B **50** 11845
[15] El Boudouti E H, Djafari-Rouhani B, Akjouj A and Dobrzynski L 1996 *Phys. Rev.* B **54** 14728
[16] Köhler R, Tredicucci A, Beltram F, Beere H E, Linfield E H, Davies A G, Ritchie D A, Iotti R C and Rossi F 2002 *Nature* **417** 156
[17] Tamura S I, Watanabe H and Kawasaki T 2005 *Phys. Rev.* B **72** 165306
[18] Trigo M, Bruchhausen A, Fainstein A, Jusserand B and Thierry-Mieg V 2002 *Phys. Rev. Lett.* **89** 227402
[19] Worlock J M and Roukes M L 2003 *Nature* **421** 802
[20] Aynaou H, El Boudouti E H, Djafari-Rouhani B, Akjouj A and Velasco V R 2005 *J. Phys.: Condens. Matter* **17** 4245
[21] Mizuno S 2002 *Phys. Rev.* B **65** 193302
[22] Lanzillotti-Kimura N D, Fainstein A, Balseiro C A and Jusserand B 2007 *Phys. Rev.* B **75** 024301
[23] Chen J J, Zhang K W, Gao J and Cheng J C 2006 *Phys. Rev.* B **73** 094307
[24] Manzanares-Martinez B and Ramos-Mendieta F 2002 *Phys. Rev.* B **66** 092302
[25] Mizuno S 2003 *Phys. Rev.* B **68** 193305
[26] Gao J and Cheng J C 2007 *Appl. Phys. Lett.* **90** 111908
[27] Wang C and Barrio R A 1988 *Phys. Rev. Lett.* **61** 191
[28] Merlin R, Bajema K, Clarke R, Juang F Y and Bhattacharya P K 1985 *Phys. Rev. Lett.* **55** 1768
[29] Hsueh W J, Lin J C and Chen H C 2007 *J. Phys.: Condens. Matter* **19** 266007
[30] Hsueh W J and Chen H C 2007 *Phys. Rev.* E **76** 057701
[31] Mayeda W 1972 *Graph Theory* (New York: Wiley)